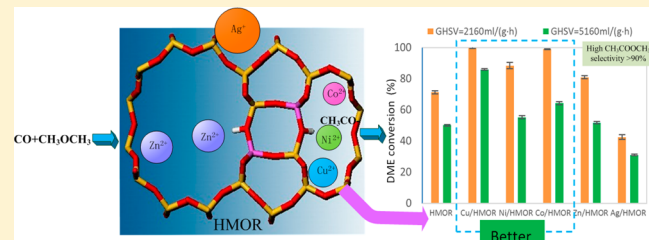


Methyl Acetate Synthesis from Dimethyl Ether Carbonylation over Mordenite Modified by Cation Exchange

Shurong Wang,* Wenwen Guo, Lingjun Zhu, Haixia Wang, Kunzan Qiu,* and Kefa Cen

State Key Laboratory of Clean Energy Utilization, Zhejiang University, Zheda Road 38, Hangzhou 310027, China

ABSTRACT: Various metal-modified HMOR catalysts for the carbonylation of dimethyl ether (DME) were prepared by ion exchange with Cu, Ni, Co, Zn, or Ag. The catalysts were characterized by the Brunauer–Emmett–Teller method, X-ray diffraction measurements, transmission electron microscopy, X-ray photoelectron spectroscopy, nuclear magnetic resonance spectroscopy, temperature-programmed desorption of ammonia, and temperature-programmed oxidation. We found that the pore structure of mordenite (HMOR) was well maintained and that the metal species were highly dispersed on the zeolite. On HMOR subjected to ion exchange with Cu, Ni, Co, or Zn, the metal ions were mainly at the zeolite exchange sites with some corresponding metal oxides. Some Brønsted acid sites were converted to Lewis acid sites, and some strong acid sites were formed together. HMOR modified with Cu, Ni, or Co showed good catalytic performance, with Cu/HMOR exhibiting the highest performance. DME conversion and methyl acetate selectivity were close to 100% under the optimum reaction conditions, which is attributed to the joint participation of Brønsted acid sites contributing to DME conversion and metal Lewis acid sites contributing to CO binding, along with the appropriate coordination structure. Modification with Cu not only improved the catalytic activity, but also suppressed carbon deposition and extended the catalyst lifetime.



1. INTRODUCTION

Methyl acetate (MA) is an ideal precursor for the synthesis of ethanol, as the latter can be obtained simply by MA hydrogenation.^{1,2} Ethanol can be easily used as a drop-in fuel, so it is an attractive liquid fuel.³ Generally, MA is produced by the esterification of acetic acid with methanol. Acetic acid is produced chiefly by methanol carbonylation⁴ based on the Cativa process developed by BP Chemicals. This process uses an iridium-based catalyst and iodomethane as a promoter. Dimethyl ether (DME) can be directly synthesized from abundant biomass,⁵ the carbonylation of which is also an effective route for MA production. Catalysts for this route include zeolites and heteropolyacids.^{6,7}

Recently, zeolites such as H-BEA, ferrierite, and especially mordenite (HMOR) were found to be active in MA synthesis by DME carbonylation.^{8,9} The selectivity of MA synthesis over HMOR is as high as 90%; however, the DME conversion needs improvement, especially at high-space-velocity conditions.^{10–12} Li et al.¹⁰ studied DME carbonylation over HZSM-35 zeolites that had been treated by alkaline solutions of different concentrations. A DME conversion of 43.6% was obtained under the following reaction conditions: gas hourly space velocity (GHSV) of 0.13 h⁻¹, temperature (*T*) of 220 °C, pressure (*P*) of 2.0 MPa, and CO/DME mole ratio [*n*(CO)/*n*(DME)] = 10.0. Xue et al.¹² obtained a higher DME conversion (38%) over nanometer-sized mordenite (at a DME/CO/He ratio of 5/76/19, a flow rate of 8.34 mL/min and a catalyst loading amount of 0.1 g) than over micrometer-sized mordenite. The carbonylation activity of zeolites depends closely on their acid sites.⁹ Other investigations have revealed

that metal-ion exchange can be used to modify the acidity and acid distribution of zeolites and thus to achieve good catalytic performance. García-Treco and Martínez¹³ prepared samples with different amounts of Brønsted acid sites and Lewis acid sites by partial exchange of protons with Na⁺ and Co²⁺. Fei et al.¹⁴ prepared Fe-, Co-, Ni-, Cr-, and Zr-modified HY zeolites to synthesize DME by methanol dehydration. They found that Fe-, Co-, and Cr-modified HY zeolites contained higher proportions of strong acid sites, whereas Zr- and Ni-modified HY zeolites had lower proportions of strong acid sites, leading to their increased stability.

Therefore, zeolites whose acid strengths are modulated by partial ion-exchange with Cu, Co, Ni, Zn, or Ag have great potential for use in DME carbonylation. The introduction of metal ions enables the adsorption of greater amounts of CO. Because the diameters of Cu²⁺, Co²⁺, Ni²⁺, Zn²⁺, and Ag⁺ are different, these ions coordinate in different HMOR channels, leading to differences in catalytic performance. In the present study, we prepared Cu-, Ni-, Co-, Zn-, and Ag-modified HMOR for DME carbonylation by the cation-exchange method. We obtained structural information on the active sites of the catalysts by characterization. Finally, we compared the stabilities of HMOR and the catalyst with the best performance.

Received: November 18, 2014

Revised: December 9, 2014

Published: December 10, 2014

Table 1. Textural Properties of the Samples

sample	EFAl ^a (%)	actual metal content (%)	S_{BET} (m^2/g)	$S_{\text{micropore}}$ (m^2/g)	V_{pore} (mL/g)	$V_{\text{micropore}}$ (mL/g)	D_{pore} (nm)
HMOR	17.1	—	416	364	0.27	0.19	2.6
Cu/HMOR	7.0	1.74	391	365	0.30	0.18	3.1
Ni/HMOR	9.2	1.30	385	354	0.28	0.18	2.8
Co/HMOR	10.0	1.36	351	323	0.27	0.16	3.0
Zn/HMOR	7.8	1.67	389	365	0.27	0.18	2.8
Ag/HMOR	8.6	1.64	376	351	0.27	0.18	2.9

^aExtraframework aluminum atoms (EFAl) as determined by ^{27}Al MAS NMR spectroscopy.

2. EXPERIMENTAL SECTION

2.1. Catalyst Preparation. HMOR ($\text{SiO}_2/\text{Al}_2\text{O}_3 = 18$) was purchased from Tosoh Catalyst Plant (Tosoh Co., Tokyo, Japan). All nitrates were purchased from Sinopharm Chemical Reagent Co. Ltd. The catalysts were prepared by the ion-exchange method. First, 0.02 mol/L $\text{Cu}(\text{NO}_3)_2$ solution was prepared, and HMOR was added to this solution to form a suspension. After the suspension had been stirred for 24 h, it was filtered, washed with excess deionized water several times, and then dried at 110 °C overnight. The final sample was calcined at 500 °C for 5 h in air. The prepared catalysts labeled as Cu/HMOR, Ni/HMOR, Co/HMOR, Zn/HMOR, and Ag/HMOR were prepared in the same way. It is important to note that, for Ag/HMOR, the procedure was performed in the dark because of the sensitivity of silver to light. The amount of metal in each catalyst was analyzed by inductively coupled plasma atomic emission spectroscopy (ICP-AES; Thermo Fisher, iCAP 6000).

2.2. Catalyst Characterization. **2.2.1. Inductively Coupled Plasma Atomic Emission Spectroscopy (ICP-AES).** To analyze the actual amounts of metal in the prepared catalysts, ICP-AES analysis was carried out. Catalyst was added to reverse aqua regia (HNO_3/HCl in a volume ratio of 3:1), and the mixture was digested with the aid of microwave radiation. The amount of each element was then determined by ICP-AES.

2.2.2. Brunauer–Emmett–Teller (BET) Method. To study the pore structures of the catalysts, the physical adsorption of nitrogen by the catalysts was tested. Before each test, the sample was degassed at 300 °C for 3 h. N_2 adsorption–desorption isotherms were recorded at –196 °C using an automated surface area and pore size analyzer (Quantachrome, Quadasorb SI). The specific surface area was calculated according to the multipoint BET method. The micropore specific surface area was calculated according to the *t*-plot method. The pore-size distribution was determined from the adsorption branches of the adsorption isotherms by the Barrett–Joyner–Halenda (BJH) method.

2.2.3. X-ray Diffraction (XRD). To investigate the crystal structure, catalysts were characterized using a D/max-Ra X-ray diffractometer with $\text{Cu K}\alpha$ radiation. The diffractometer was operated at 40 kV and 30 mA. Scans were recorded from 5° to 80° at a step width of 0.016° and a collecting time of 5 s.

2.2.4. Transmission Electron Microscopy (TEM). To explore the particle size and distribution of catalysts, TEM (Philips-FEI, Tecnai G2 F30) was performed.

2.2.5. X-ray Photoelectron Spectroscopy (XPS). To study the chemical state of metallic species, XPS was carried out. XPS and X-ray Auger electron spectroscopy were performed on a PHI 5000C ESCA system equipped with a Mg $\text{K}\alpha$ X-ray radiation source ($h\nu = 1253.6$ eV). Binding energies were

calibrated with respect to the C 1s peak at 284.6 eV with an uncertainty of ±0.2 eV.

2.2.6. Nuclear Magnetic Resonance (NMR) Spectroscopy. To obtain information on the coordination of Al and Si species, NMR experiments for ^{27}Al and ^{29}Si were performed on a Bruker AV-400 WB spectrometer at resonance frequencies of 104.3 and 79.5 MHz, respectively. Magic-angle-spinning solid-state NMR spectra for ^{27}Al and for ^{29}Si were recorded at spinning rates of 12 and 4 kHz, respectively.

2.2.7. Temperature-Programmed Desorption of Ammonia (NH_3 TPD) and Temperature-Programmed Oxidation (TPO). To monitor the acid strengths and the amounts of acid sites in the samples, NH_3 TPD was performed on an AutoChem II instrument. A 50-mg sample was preheated in He at 500 °C for 1 h, and then NH_3 adsorption was performed at 120 °C for 1 h. Subsequently, the sample was flushed with He for 1.0 h at 120 °C to remove physically adsorbed NH_3 . NH_3 desorption was carried out by increasing the temperature to 700 °C at a heating rate of 10 °C/min. A mass spectrometer was used to obtain the corresponding NH_3 desorption profiles. TPO was carried out on the same instrument, and a thermal conductivity detector (TCD) was used to detect the O_2 consumption signal. Samples were heated to 900 °C at a ramping rate of 5 °C/min under a flow of a 2% O_2/He mixture at 30 mL/min.

2.3. Catalyst Evaluation. Catalytic tests were performed in a fixed-bed reactor. The catalyst loading was 500 mg. Quartz sand was packed under the catalyst. First, the temperature was raised to 210 °C, and the pressure was raised to 1.8 MPa. A CO/DME/ N_2 mixture [volume ratio of $V(\text{CO})/V(\text{DME}) = 19.0$, flow rate of $V(\text{N}_2) = 3.0$ mL/min] was then introduced into the reactor. All products were analyzed by online gas chromatography (GC; Huai GC 9560). The oven temperature was maintained at 50 °C for 9 min and then increased to 180 °C at a ramp rate of 10 °C/min, afterwards was held at 180 °C for 3 min. CO, CO_2 , and N_2 were separated by a TDX-01 packed column and then detected by TCD, while the gaseous hydrocarbons and oxygenates (DME, methanol, MA, etc.) were separated by a Propack-Q packed column and then detected by flame ionization detector (FID). To prevent product condensation, the reactor effluent was injected into the GC system through transfer lines held at 180 °C. We employed a GC method based on internal calibration to determine the product yield. Nitrogen was used as the internal gas, as is commonly done in quantitative analysis. The nitrogen does not participate in and has little influence on the reaction. The average correction factors of all species relating to N_2 were measured before the reaction, and the flow rate of N_2 was fixed at 3.0 mL/min during the reaction. Therefore, the quantities of the products could be calculated based on their peak areas and the corresponding correction factors. The DME conversion (X_{DME}) was calculated according to the equation

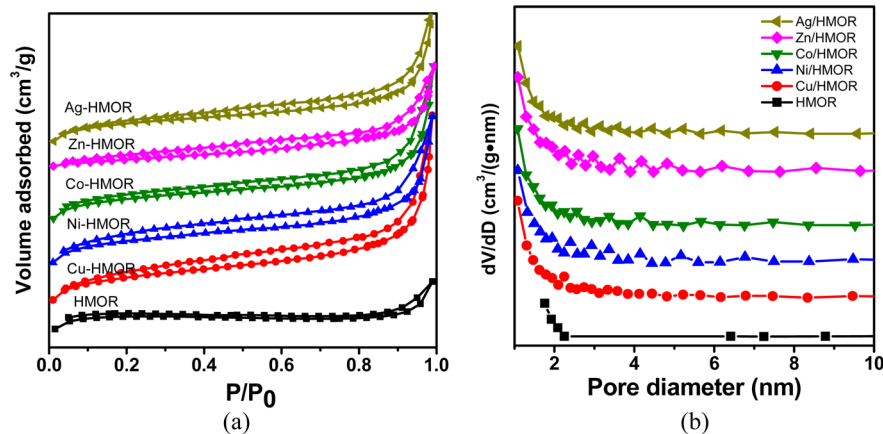


Figure 1. (a) N₂ adsorption–desorption isotherms and (b) pore-size distributions of the samples.

$$X_{\text{DME}} (\%) = \left(\frac{n_{\text{DME}_{\text{in}}} - n_{\text{DME}_{\text{out}}}}{n_{\text{DME}_{\text{in}}}} \right) \times 100\% \quad (1)$$

where $n_{\text{DME}_{\text{in}}}$ and $n_{\text{DME}_{\text{out}}}$ represent the numbers of moles of DME in the feed and vent gas, respectively.

The equation for MA synthesis from DME is



For the synthesis of 1 mol of MA from 1 mol of DME, the equation for MA selectivity (S_{MA}) is

$$S_{\text{MA}} (\%) = \left(\frac{\text{moles of MA produced}}{\text{moles of DME converted}} \right) \times 100\% \quad (2)$$

3. RESULTS

3.1. Catalyst Characterization. 3.1.1. Structural Analysis.

The metal contents and textural properties of the six samples investigated are listed in Table 1. The nitrate solutions used in catalyst preparation were identical (0.02 mol/L), but the metal contents varied slightly (from 1% to 2%). The BET surface area and micropore area of HMOR were found to be 416 and 364 m²/g, respectively. After partial exchange with metal ions, the BET surface area decreased slightly, and the pore diameter and pore volume increased slightly. These changes can be attributed to the formation of new pores. Figure 1a displays N₂ adsorption–desorption isotherms of the samples. The adsorption isotherm of HMOR is of type I. After exchange of HMOR with metal ions, hysteresis of the isotherm appeared earlier, tending toward an isotherm of type II. This trend indicates the formation of new mesopores. This trend can be also seen in Figure 1b: Micropores were retained, and new mesopores were generated.

3.1.2. XRD. Figure 2 displays the XRD patterns of the samples. The samples used were highly crystalline, and the cation-exchange method did not affect the crystal structure of the zeolite. Diffraction peaks at 2θ values of 9.2°, 20.5°, and 23.6° are typical of HMOR XRD patterns.¹⁵ No shift in peak positions and no significant diffraction lines attributed to any new phase could be observed in the patterns of HMOR after being subjected to metal-ion exchange. These observations can be attributed to the low metal contents used (1–2%), the small particle size (<3 nm), and the high dispersion of metal species in the zeolite framework.¹⁶

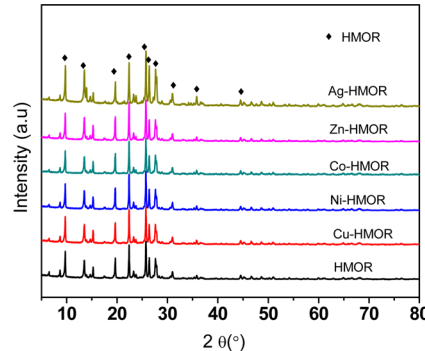


Figure 2. XRD patterns of the samples.

3.1.3. TEM. Figure 3 shows TEM images of the prepared catalysts. Figure 3a1 displays a TEM image of Cu/HMOR catalyst. The copper species were evenly dispersed, and the observed particle size was about 2–3 nm. The interplanar distance of 0.275 nm corresponds to CuO(110) (Figure 3a2), revealing the presence of CuO in the Cu/HMOR catalyst. TEM images of Ni/HMOR (Figure 3b1,b2) show that the nickel species were well-dispersed in the HMOR framework. Lattice fringes (0.209 nm) corresponding to NiO(200) indicate the presence of NiO in Ni/HMOR. TEM images of Co/HMOR (Figure 3c1,c2) and Zn/HMOR (Figure 3d1,d2) reveal that the cobalt and zinc species were uniformly distributed in the samples. Interplanar spacings of 0.213 nm (Figure 3c2) and 0.248 nm (Figure 3d2) correspond to CoO(200) and ZnO(101), respectively. For Cu-, Co-, Ni-, and Zn-modified HMOR, the average particle sizes calculated from the TEM images were 2–3 nm. TEM images of Ag/HMOR (Figure 3e1–e4) showed markedly different morphologies. The silver species were spherical and highly dispersed and covered the HMOR surface (as seen in the edges). They had diameters of about 4–5 nm. High-magnification TEM images (Figure 3e3,e4) indicate that the spherical species consisted of Ag₂O. This finding might be due to the difficulty of exchanging Ag⁺ with the protons on HMOR. Furthermore, Ag⁺ is probably more strongly attached to the HMOR surface, resulting in the formation of Ag₂O nanoparticles on the HMOR surface.

The microstructure of Co/HMOR was examined by scanning transmission electron microscopy (STEM). Figure 4 shows an STEM image of Co/HMOR and the corresponding element maps for O, Al, Si, and Co. Bright spots in the figure corresponding to Co indicate that the Co species were well

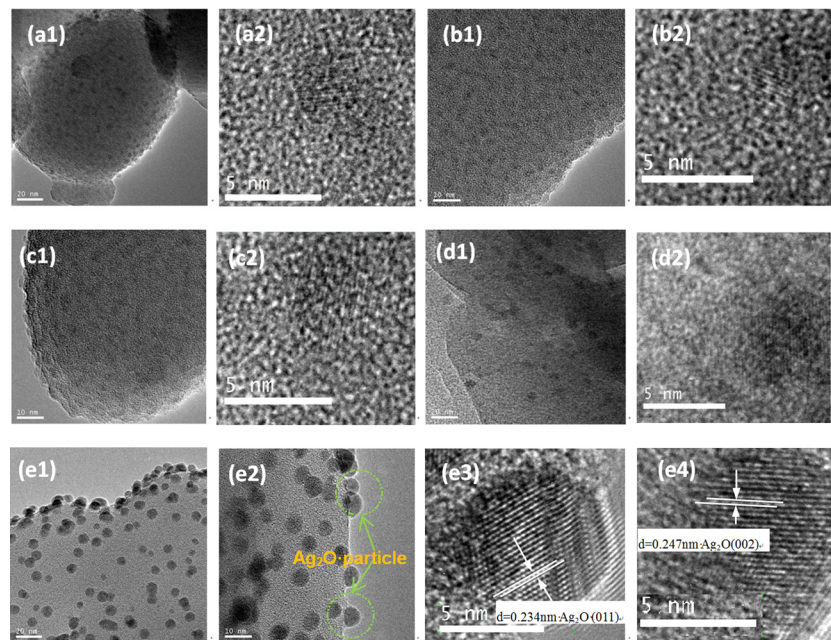


Figure 3. TEM images of the prepared catalysts: (a1,a2) Cu/HMOR, (b1,b2) Ni/HMOR, (c1,c2) Co/HMOR, (d1,d2) Zn/HMOR, and (e1–e4) Ag/HMOR.

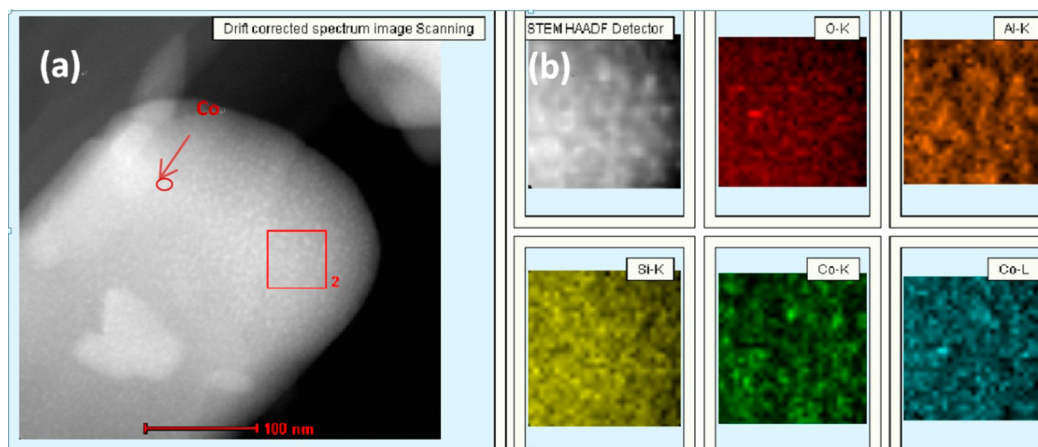


Figure 4. (a) STEM image of Co/HMOR and (b) corresponding element maps for O, Al, Si, and Co.

distributed in HMOR. As seen in the element maps (Figure 4b), O (red), Al (orange), Si (yellow), and Co (green) were uniformly dispersed in the sample.

3.1.4. XPS. The Cu 2p_{3/2} binding energy is 933.6 eV (Figure 5a), corresponding to Cu²⁺ introduced by cation exchange.¹⁷ The XPS spectrum of Ni/HMOR (Figure 5b) shows a peak centered at 857.5 eV. The binding energy, which is ~2.0 eV higher than that of NiO, is assigned to Ni²⁺ at the zeolite exchange sites.^{18,19} This difference might be due to the different coordinated states of Ni²⁺ and NiO in the zeolite. The Co 2p XPS spectrum (Figure 5c) exhibits a main peak at 785.0 eV and surrounding shakeup satellite peaks, which are characteristic of Co²⁺ species at zeolite exchange sites.²⁰ The presence of satellite peaks is often used to distinguish Co²⁺ from Co³⁺.²¹ The Zn 2p spectrum (Figure 5d) has a peak centered at 1023.3 eV, which is assigned to Zn²⁺ in Zn/HMOR.²² The Ag 3d XPS and Ag MMN spectra (Figure 5e,f) show that the Ag 3d_{5/2} and Ag 3d_{3/2} binding energies are 370.0 and 376.0 eV, respectively. Because the binding energies of Ag 3d_{5/2} in Ag₂O and Ag are close (within 0.5 eV), distinguishing them using the Ag 3d

binding energy is difficult. The modified Auger parameter, $\alpha' = E_K(\text{Ag MNN}) + E_B(\text{Ag } 3\text{d}_{5/2})$, was thus used for a more accurate determination of the chemical state of Ag. The α' value for Ag/HMOR was found to be ~723.2 eV [$E_K(\text{Ag MNN}) = 353.2$ eV]. According to the literature, binding energies of 726.3, 724.5, and 722.2 eV correspond to Ag⁰, Ag₂O, and Ag⁺, respectively.^{23–25} Therefore, the results suggest that the silver species at exchange sites in Ag/HMOR are mainly Ag₂O and Ag⁺.

3.1.5. NMR Spectroscopy. ²⁷Al NMR spectra (Figure 6A) provide information about the coordination of aluminum species. The peak at 54 ppm corresponds to tetrahedrally coordinated Al atoms in the framework, and that at -1 ppm is due to extraframework aluminum (EFAl) atoms.²⁶ EFAl comprises the Al atoms at the extraframework sites of the zeolite, which are not tetrahedrally coordinated in the framework during the crystallization process. It consists of different species, such as Al³⁺, Al(OH)₂⁺, Al(OH)²⁺, AlOOH, and Al(OH)₃. EFAl percentages are listed in Table 1. The EFAl content of HMOR is 17.1%. After ion exchange, it decreases

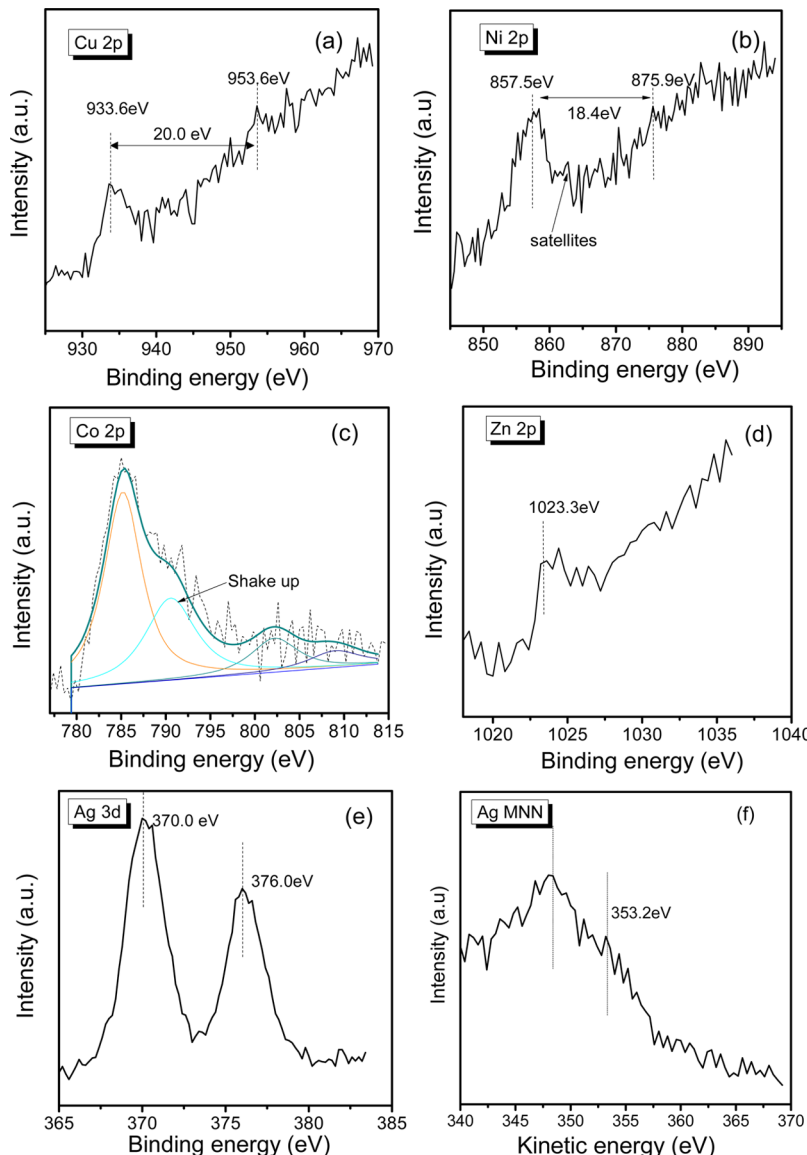


Figure 5. XPS spectra of the prepared catalysts: (a) Cu/HMOR, (b) Ni/HMOR, (c) Co/HMOR, (d) Zn/HMOR, and (e) Ag/HMOR. (f) XPS spectrum of the Ag MNN Auger region.

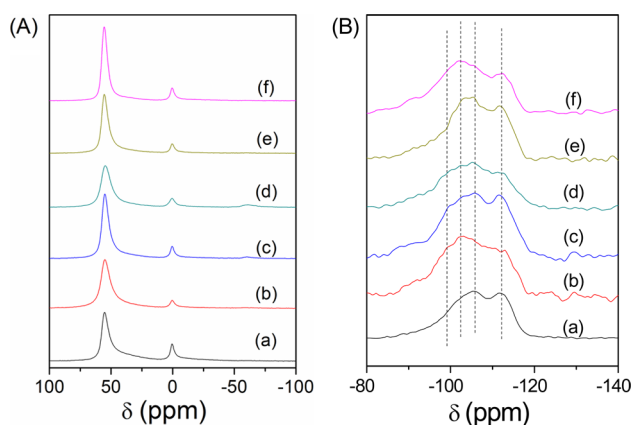


Figure 6. (A) ^{27}Al and (B) ^{29}Si MAS NMR spectra of the support and prepared catalysts: (a) HMOR, (b) Cu/HMOR, (c) Ni/HMOR, (d) Co/HMOR, (e) Zn/HMOR, and (f) Ag/HMOR.

from 17.1% to 7.1%, especially in the case of Cu/HMOR. The loss of EFAl atoms might occur during washing in catalyst preparation,²⁷ and it might result from strong interactions between metal ions and EFAl atoms.²⁸

Figure 6B displays ^{29}Si MAS NMR spectra of the samples. According to Loewenstein's rule, Al–O–Al linkages cannot exist in zeolites.²⁹ One Si atom can be coordinated by zero, one, two, three, or four Al atoms, denoted as Si(0Al), Si(1Al), Si(2Al), Si(3Al), or Si(4Al), respectively. Signals in the ^{29}Si NMR spectra of the samples (Figure 6B) at -112, -106, -103, and -99 ppm are assigned to Si(0Al), Si(0Al), Si(1Al), and Si(2Al), respectively.³⁰ Si atoms in HMOR are mainly at the Si(0Al) and Si(1Al) sites. After ion exchange, the strengths of the signals at -103 and -99 ppm increased. The presence of metal ions in the zeolite rings affects the Si coordination environment, leading to local ring distortions,³¹ which mainly affect Si atoms at the Si(1Al) and Si(2Al) sites. Hence, the intensities of the signals corresponding to Si(1Al) and Si(2Al), especially those for the Cu/HMOR catalyst, increased (Figure 6B).

3.1.6. NH_3 TPD. As shown in Figure 7, the NH_3 TPD profile of the parent HMOR presents peaks at 188 and 448 °C. The

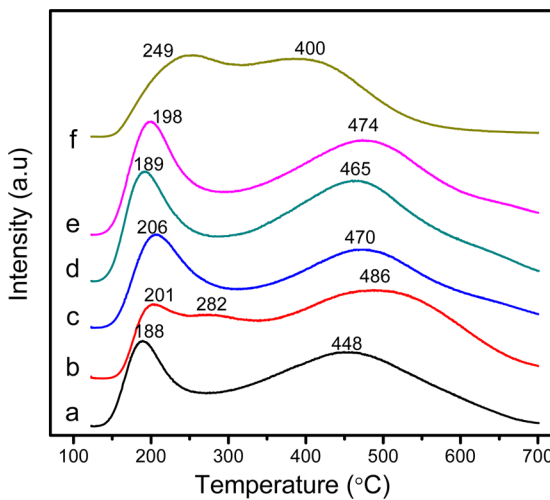


Figure 7. NH_3 TPD profiles of the prepared samples: (a) HMOR, (b) Cu/HMOR, (c) Ni/HMOR, (d) Co/HMOR, (e) Zn/HMOR, and (f) Ag/HMOR.

peak at 188 °C corresponds to NH_3 adsorbed on weak acid sites or to EFAI,³² and that at 448 °C is due to NH_3 adsorbed on strong acid (Brønsted and/or Lewis) sites.^{33,34} After ion exchange of the zeolite with metal ions (Cu^{2+} , Ni^{2+} , Co^{2+} , Zn^{2+} , or Ag^+), the positions and intensities of the peaks changed. Some Brønsted acid sites were converted to Lewis acid sites after exchange of Cu^{2+} , Ni^{2+} , Co^{2+} , Zn^{2+} , or Ag^+ with the protons of the zeolites.^{35–37} Exchanged multivalent cations could react with absorbed water or crystal water in HMOR, forming hydrous positive ions. Water polarization effects due to metal ions were enhanced during drying. This resulted in the dissociation of H^+ and the generation of new Brønsted acid sites. The role of divalent metal cations in the enhancement of the acidic strength can be explained by the mechanism of framework distortion and electron-withdrawing effects.³⁸ When the cation valences of the samples are the same, smaller cations lead to a stronger electron-accepting ability and a greater acidic strength. Hence, the acidic strength of the samples decreased in the order $\text{Zn}^{2+} > \text{Cu}^{2+} > \text{Ni}^{2+} > \text{Co}^{2+}$. The positions of the high-temperature desorption peaks showed a similar trend, except

that the high-temperature desorption peak of Cu/HMOR (486 °C) was higher than that of Zn/HMOR (474 °C). This difference might be due to local ring distortions, as seen in the ^{29}Si MAS NMR spectra. A new desorption peak at 282 °C attributed to NH_3 adsorbed on sites of medium acidity could be observed in the Cu/HMOR NH_3 TPD curve. This indicates the formation of new acidic sites. Ag/HMOR presented a homogeneous strength distribution of acidic sites, which might be due to the formation of new sites of medium acidity after Ag^+ exchange of HMOR.

3.2. Catalytic Performance. The results of DME carbonylation over the samples are shown in Figure 8. The S_{MA} values of all six samples were high (>90%), and the main byproducts were methanol and methane. However, the X_{DME} values of the six samples exhibited large differences. As shown in the figure, the catalytic performances of Cu-, Co-, and Ni-modified HMOR were better than that of HMOR, the catalytic performances of Zn/HMOR and HMOR were similar, and the performance of Ag/HMOR was lower than that of HMOR. At GHSV = 2160 mL/(g·h), the X_{DME} values over Cu/HMOR and Co/HMOR were close to 100%. To distinguish their conversion capacities, the GHSV was increased from 2160 to 5160 mL/(g·h). In this case, the X_{DME} and S_{MA} values over Cu/HMOR were 86.0% and 99.6%, respectively; those over Co/HMOR decreased to 64.3% and 99.4%, respectively; and those over Ni/HMOR were 55.3% and 98.7%, respectively. All of these values were higher than those of HMOR (50.1% and 97.3%, respectively). The catalytic performance of Zn/HMOR was similar to that of HMOR. The X_{DME} value over Ag/HMOR was as low as 32.1%, and the S_{MA} value was 94.3%. This might be due to the decrease in the acid strength after the introduction of Ag and the decrease in the amount of active sites covered by Ag_2O .

The influence of the GHSV on the X_{DME} and S_{MA} values over Cu/HMOR was also studied, as shown in Figure 9. As the GHSV was increased, the X_{DME} and S_{MA} values decreased because of the short residence time. When the GHSV increased from 2160 to 3960 mL/(g·h) (nearly doubled), the X_{DME} value decreased slightly from 99.9% to 93.7%. When the GHSV was further increased, X_{DME} decreased rapidly. The optimal GHSV was probably in the range of 2160–5160 mL/(g·h).

The stabilities of HMOR and the catalyst with the highest performance (Cu/HMOR) were analyzed at 210 °C, 1.8 MPa, and 3960 mL/(g·h) GHSV, as displayed in Figure 10. The

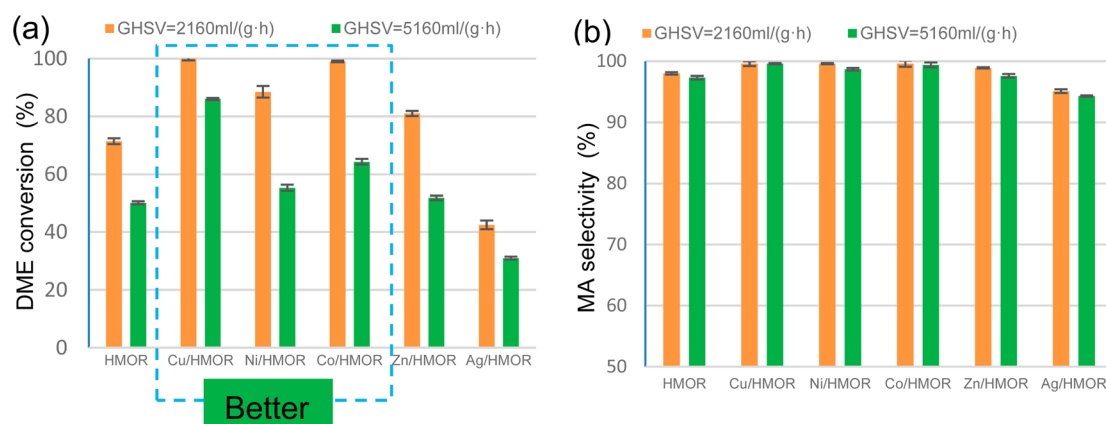


Figure 8. (a) DME conversions and (b) MA selectivities over different mordenite catalysts subjected to metal-ion exchange at steady state. Reaction conditions: $T = 210$ °C, $P = 1.8$ MPa, $V(\text{N}_2) = 3.0$ mL/min, $n(\text{CO})/n(\text{DME}) = 19.0$.

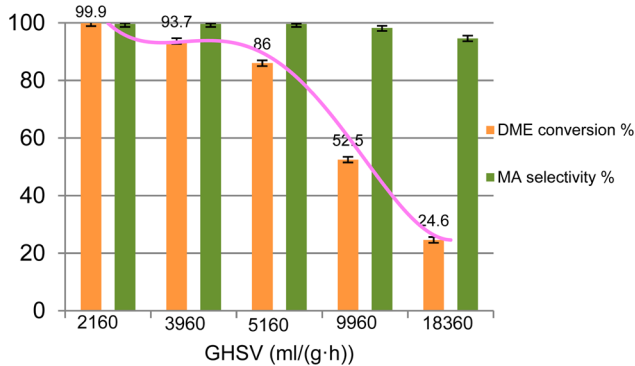


Figure 9. Influence of GHSV on MA selectivity and DME conversion over Cu/HMOR at steady state. Reaction conditions: $T = 210\text{ }^{\circ}\text{C}$, $P = 1.8\text{ MPa}$, $V(\text{N}_2) = 3.0\text{ mL/min}$, $n(\text{CO})/n(\text{DME}) = 19.0$.

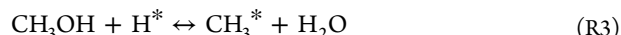
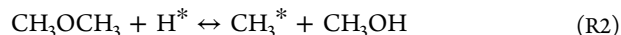
induction period for the two catalysts was 3 h. During the induction period, the X_{DME} value increased until it reached steady state. At steady state, the X_{DME} values over Cu/HMOR and HMOR were 93.7% and 53.6%, respectively, and the S_{MA} values over Cu/HMOR and HMOR were 99.6% and 97.4%, respectively. Methanol was the main byproduct. After a steady-state period of ~ 1.5 h during the 10-h test, the X_{DME} value of HMOR decreased rapidly from 52.7% to 24.1%, the S_{MA} value decreased from 97.4% to 66.3%, and the main byproducts were methane and methanol. Over Cu/HMOR, the steady-state period was ~ 2.5 h, after which the X_{DME} value decreased to 65.5%, and the S_{MA} value remained almost unchanged.

4. DISCUSSION

Ion exchange in aqueous solution led to good dispersion of the metal ions in the zeolite framework and did not affect the crystal structure of the zeolite. On HMOR subjected to ion exchange with Cu, Ni, Co, and Zn, the metal ions were mainly at the zeolite exchange sites with some corresponding metal oxides. On Ag/HMOR, appreciable quantities of Ag appeared as spherical Ag_2O nanoparticles, covering the surface of HMOR.

DME carbonylation involves the formation of methyl groups and methanol through a quasi-equilibrated reaction of DME with acidic protons (mainly Brønsted acidic).⁹ CH_3OH then reacts with another acidic proton to form water and methyl groups. This process is called the induction period at the early stage of the reaction, which yields the byproduct methanol. As

more methyl groups form, CO reacts with the methyl groups, thereby forming acetyl species. MA forms through the reaction of acetyl species with methyl groups^{9,39}



The key reaction step of DME carbonylation is the insertion of CO into a methyl group.^{39,40} For HMOR, the EFAI atoms act as Lewis acid sites for binding CO.^{41,42} After ion exchange, new metal Lewis acid sites form, providing more sites for binding CO.⁴³ Thus, the key reaction step is promoted, facilitating DME conversion. Therefore, an appropriate carbonylation catalyst requires the joint participation of Brønsted acid sites and metal Lewis acid sites. HMOR contains both sites, with the Lewis acid sites being derived from EFAI atoms. After ion exchange, some Brønsted acid sites are converted to metal Lewis acid sites, and some new sites of strong acidity are formed. Sites of medium acidity also form on copper-modified HMOR. As the metal ions differ in diameter, they tend to coordinate to different HMOR channels. In their investigation of the coordination of divalent metal cations to ZSM-5 using gradient-corrected density functional theory, Rice et al.⁴⁴ found that Cu^{2+} , Co^{2+} , Fe^{2+} , and Ni^{2+} coordinate preferentially to five-membered rings, whereas Zn^{2+} coordinates preferentially to six-membered rings. This finding suggests that the metal ions in our study coordinate preferentially to different rings in HMOR. The reaction mechanisms of DME carbonylation in the 8- and 12-membered ring channels of HMOR are different.⁴⁵ The former channel is where the acetyl intermediate of DME carbonylation mainly forms. Because the X_{DME} value over Zn/HMOR is similar to that over HMOR and because of the large radius of Zn^{2+} , Zn^{2+} probably exchanges with protons in the 12-membered rings. As the radii of Cu^{2+} , Co^{2+} , and Ni^{2+} are smaller, they tend to exchange with protons in the eight-membered rings. Acid sites over Ag/HMOR, however, have a homogeneous strength distribution, and Ag_2O covers some active sites, which does not favor DME conversion, leading to an inferior catalytic performance. The structures of various metal ions coordinated in HMOR channels are presented in Figure 11.

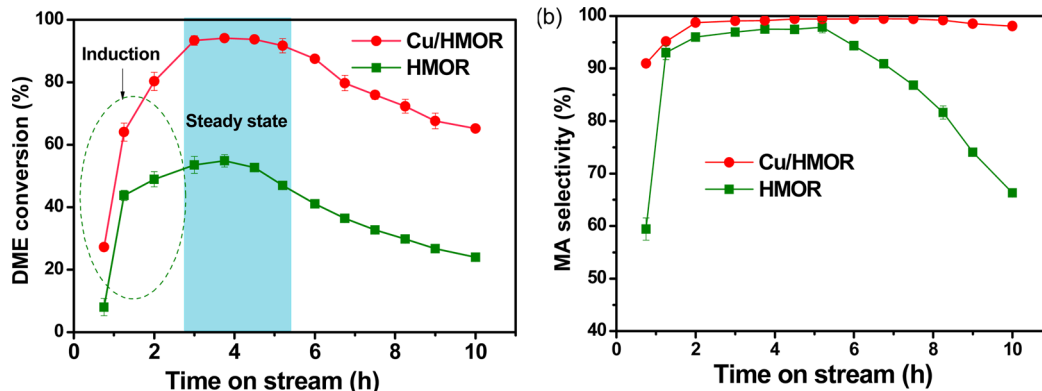


Figure 10. (a) DME conversions and (b) MA selectivities over HMOR and Cu/HMOR catalysts with time on stream. Reaction conditions: $T = 210\text{ }^{\circ}\text{C}$, $P = 1.8\text{ MPa}$, GHSV = 3960 mL/(g·h), $V(\text{N}_2) = 3.0\text{ mL/min}$, $n(\text{CO})/n(\text{DME}) = 19.0$.

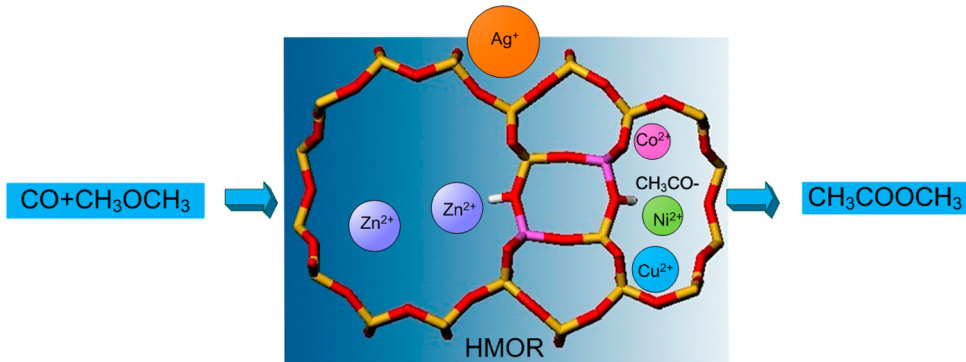


Figure 11. Structures of various metal ions coordinated in HMOR channels.

Hydrocarbons formed during the reaction play the main role in catalyst deactivation by blocking the catalyst channels. During DME carbonylation, surface methoxy groups react with DME to form trimethyl oxonium cations, which can subsequently react to yield hydrocarbons.⁴⁶ Figure 12 displays

5. CONCLUSIONS

Various catalysts for DME carbonylation were prepared by ion exchange of HMOR with Cu²⁺, Ni²⁺, Co²⁺, Zn²⁺, and Ag⁺. On HMOR subjected to ion exchange with Cu, Ni, Co, or Zn, the metal ions were mainly at the zeolite exchange sites with some corresponding metal oxides. Addition of Cu, Ni, and Co species to HMOR increased the acid strength of the catalyst and enhanced DME conversion. Among the catalysts, Cu/HMOR showed the best performance, as it contained proper amounts of Brønsted acid sites for DME conversion and metal Lewis acid sites for binding CO, as well as the appropriate coordination structure. At reaction conditions of $T = 210\text{ }^{\circ}\text{C}$, $P = 1.8\text{ MPa}$, and GHSV = 2160 mL/(g·h), the X_{DME} and S_{MA} values over Cu/HMOR were close to 100%. When the GHSV was increased to 5160 mL/(g·h), the X_{DME} and S_{MA} values were 86.0% and 99.6%, respectively, whereas the X_{DME} value over HMOR under the same reaction conditions was 50.1%. Cu-modified HMOR also suppressed byproduct formation and extended the catalyst life. Zn²⁺ probably exchanged with protons in the 12-membered rings of HMOR, resulting in an X_{DME} value similar to that of HMOR. Ag-modified HMOR presented a homogeneous acid strength distribution, which led to a low X_{DME} value.

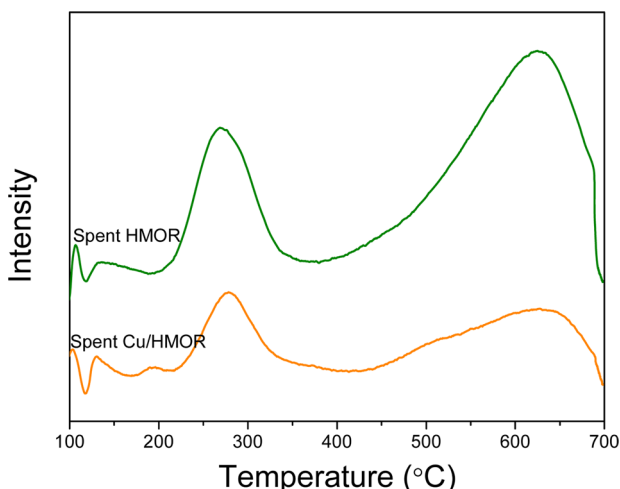


Figure 12. TPO profiles of the spent catalysts.

TPO profiles of the spent catalysts. The two curves present two peaks at 268 and 621 °C, which indicate two carbon species formed after the reaction. The peak at 268 °C is attributed to the oxidation of soft coke, which is composed of reaction intermediates, namely, surface-bound methyls and acetals associated with the formation of MA. The peak at 621 °C is ascribed to the oxidation of heavy coke,⁴⁷ which mainly consists of large hydrocarbons. Heavy coke hinders reactant diffusion, thereby leading to catalyst deactivation. The significantly lower intensity of the high-temperature peak of Cu/HMOR compared with that of HMOR suggests that less coke formed during the reaction on Cu/HMOR. This reduction might be due to the formation of new metal Lewis acid sites over Cu-modified HMOR that provide new sites to bind CO, suppress hydrocarbon formation, and inhibit catalyst deactivation. After the steady state, the rapid decrease of S_{MA} from 97.4% to 66.3% over unmodified HMOR was due to serious catalyst deactivation, whereas the MA selectivity over Cu-modified HMOR remained almost unchanged, as seen in Figure 10.

■ AUTHOR INFORMATION

Corresponding Authors

*E-mail: srwang@zju.edu.cn. Tel.: +86 571 87952801. Fax: +86 571 87951616.

*E-mail: qiuqz@zju.edu.cn. Tel.: +86 571 87952066. Fax: +86 571 87951616.

Notes

The authors declare no competing financial interest.

■ ACKNOWLEDGMENTS

We acknowledge financial support from the National Natural Science Foundation of China (51276166), the National Science and Technology Supporting Plan through Contract 2015BAD15B06, and the Program of Introducing Talents of Discipline to University (B08026).

■ REFERENCES

- (1) Yi, Z.; Xiao, G. S.; Tsubaki, N.; Tan, Y. S.; Chen, J. F. Novel Ethanol Synthesis Method via C1 Chemicals without Any Agriculture Feedstocks. *Ind. Eng. Chem. Res.* **2010**, *49*, 5485–5488.
- (2) Wang, D.; Yang, G. H.; Ma, Q. X.; Yoneyama, Y.; Tan, Y. S.; Han, Y. Z.; Tsubaki, N. Facile Solid-State Synthesis of Cu–Zn–O Catalysts

- for Novel Ethanol Synthesis from Dimethyl Ether (DME) and Syngas ($\text{CO} + \text{H}_2$). *Fuel* **2013**, *109*, 54–60.
- (3) Zuo, Z. J.; Wang, L.; Yu, L. M.; Han, P. D.; Huang, W. Experimental and Theoretical Studies of Ethanol Synthesis from Syngas over CuZnAl Catalysts without Other Promoters. *J. Phys. Chem. C* **2014**, *118*, 12890–12898.
- (4) Jones, J. H. The Cativa Process for the Manufacture of Acetic Acid. *Platinum Met. Rev.* **2002**, *44*, 94–105.
- (5) Zhu, Y. Y.; Wang, S. R.; GE, X. L.; Luo, Z. Y.; Cen, K. F. Experimental Study of Improved Two Step Synthesis for DME Production. *Fuel Process. Technol.* **2010**, *91*, 424–429.
- (6) Volkova, G. G.; Plyasova, L. M.; Salanov, A. N.; Kustova, G. N.; Yurieva, T. M.; Likhlobov, V. A. Heterogeneous Catalysts for Halide-Free Carbonylation of Dimethyl Ether. *Catal. Lett.* **2002**, *80*, 175–179.
- (7) Mikhail, V. L.; Maxim, S. K.; Galina, G. V.; Alexander, G. S. Solid-State NMR Study of the Kinetics and Mechanism of Dimethyl Ether Carbonylation on Cesium Salt of 12-Tungstophosphoric Acid Modified with Ag, Pt, and Rh. *J. Catal.* **2013**, *308*, 250–257.
- (8) Cheung, P.; Bhan, A.; Glenn, J. S.; Iglesia, E. Selective Carbonylation of Dimethyl Ether to Methyl Acetate Catalyzed by Acidic Zeolites. *Angew. Chem., Int. Ed.* **2006**, *45*, 1617–1620.
- (9) Cheung, P.; Bhan, A.; Glenn, J. S.; David, J. L.; Iglesia, E. Site Requirements and Elementary Steps in Dimethyl Ether Carbonylation Catalyzed by Acidic Zeolites. *J. Catal.* **2007**, *245*, 110–123.
- (10) Li, X. J.; Liu, X. H.; Liu, S. L.; Xie, S. J.; Zhu, X. X.; Chen, F. C.; Xu, L. Y. Activity Enhancement of ZSM-35 in Dimethyl Ether Carbonylation Reaction through Alkaline Modifications. *RSC Adv.* **2013**, *3*, 16549–16557.
- (11) Liu, J. L.; Xue, H. F.; Huang, X. M.; Li, Y.; Shen, W. J. Dimethyl Ether Carbonylation to Methyl Acetate over HZSM-35. *Catal. Lett.* **2010**, *139*, 33–37.
- (12) Xue, H. F.; Huang, X. M.; Ditzel, E.; Zhan, E. S.; Ma, M.; Shen, W. J. Coking on Micrometer and Nanometer Sized Mordenite during Dimethyl Ether Carbonylation to Methyl Acetate. *Chin. J. Catal.* **2013**, *34*, 1496–1503.
- (13) García-Trencó, A.; Martínez, A. Direct Synthesis of DME from Syngas on Hybrid CuZnAl/ZSM-5 Catalysts: New Insights into the Role of Zeolite Acidity. *Appl. Catal. A* **2012**, *411–412*, 170–179.
- (14) Fei, J. H.; Hou, Z. Y.; Zhu, B.; Lou, H.; Zheng, X. M. Synthesis of Dimethyl Ether (DME) on Modified HY Zeolite and Modified HY Zeolite-Supported Cu–Mn–Zn Catalysts. *Appl. Catal. A* **2006**, *304*, 49–54.
- (15) Lin, X.; Kikuchi, E.; Matsukata, M. Preparation of Mordenite Membranes on α -Alumina Tubular Supports for Pervaporation of Water–Isopropyl Alcohol Mixtures. *Chem. Commun.* **2000**, *11*, 957–958.
- (16) Wang, S. R.; Guo, W. W.; Wang, H. X.; Zhu, L. J.; Qiu, K. Z. Influence of Mn Promotion on CO Hydrogenation over Rh/CNTs Catalyst. *Catal. Lett.* **2014**, *144*, 1305–1312.
- (17) Kong, X. J.; Chen, L. G. Hydrogenation of Aromatic Aldehydes to Aromatic Hydrocarbons over Cu-HZSM-5 Catalyst. *Catal. Commun.* **2014**, *57*, 45–49.
- (18) Kónya, Z.; Vesselényi, I.; Kiss, J.; Farkas, A.; Oszkó, A.; Kiricsi, I. XPS Study of Multiwall Carbon Nanotube Synthesis on Ni-, V-, and Ni, V-ZSM-5 Catalysts. *Appl. Catal. A* **2004**, *260*, 55–61.
- (19) Velu, S.; Suzuki, K.; Vijayaraj, M.; Barman, S.; Chinnakonda, S. G. In Situ XPS Investigations of $\text{Cu}_{1-x}\text{Ni}_x\text{ZnAl}$ -Mixed Metal Oxide Catalysts Used in the Oxidative Steam Reforming of Bio-ethanol. *Appl. Catal. B* **2005**, *55*, 287–299.
- (20) da Cruz, R. S.; Mascarenhas, A. J. S.; Andrade, H. M. C. Co-ZSM-5 Catalysts for N_2O Decomposition. *Appl. Catal. B* **1998**, *18*, 223–231.
- (21) Li, B.; Wang, H.; Ding, F. C.; Li, C. Q.; Song, Y. J.; Ke, M.; Ren, C. T. Effects of Preparation Methods on the Catalytic Performance of Selective Catalytic Reduction of NO with CH_4 over Co-MOR Catalysts. *Acta Phys.-Chim. Sin.* **2013**, *29*, 1289–1296.
- (22) Anand, R.; Hegde, S. G.; Rao, B. S.; Gopinath, C. S. Catalytic Synthesis of 2-Methyl Pyrazine over Zn-Modified Zeolites. *Catal. Lett.* **2002**, *84*, 265–272.
- (23) Bera, S.; Gangopadhyay, P.; Nair, K. G. M.; Panigrahi, B. K.; Narasimhan, S. V. Electron Spectroscopic Analysis of Silver Nanoparticles in a Soda-Glass Matrix. *Elec. J. Spectr. Rel. Phen.* **2006**, *152*, 91–95.
- (24) Soledad, G. A.; Ramiro, M. S.; Eduardo, E. M.; Alicia, V. B. AgNaMordenite Catalysts for Hydrocarbon Adsorption and de NO_x Processes. *Appl. Catal. A* **2011**, *407*, 134–144.
- (25) Traversa, E.; Di Vona, M. L.; Nunziante, P.; Licoccia, S. Photoelectrochemical Properties of Sol-Gel Processed Ag-TiO₂ Nanocomposite Thin Films. *J. Sol-Gel Sci. Techn.* **2001**, *22*, 115–123.
- (26) Li, X. F.; Prins, R.; Bokhoven, J. A. V. Synthesis and Characterization of Mesoporous Mordenite. *J. Catal.* **2009**, *262*, 257–265.
- (27) Sun, Y.; Campbell, S. M.; Lunsford, J. H.; Lewis, G. E.; Palke, D.; Tau, L. M. The Catalytic Conversion of Methyl Chloride to Ethylene and Propylene over Phosphorus-Modified Mg-ZSM-5 Zeolites. *J. Catal.* **1993**, *143*, 32–44.
- (28) Mao, D. S.; Yang, W. M.; Xia, J. C.; Zhang, B.; Song, Q. Y.; Chen, Q. L. Highly Effective Hybrid Catalyst for the Direct Synthesis of Dimethyl Ether from Syngas with Magnesium Oxide-Modified HZSM-5 as a Dehydration Component. *J. Catal.* **2005**, *230*, 140–149.
- (29) Liu, W.; Xu, Y.; Wong, S. T.; Wang, L.; Qiu, J.; Yang, N. Methane Dehydrogenation and Aromatization in the Absence of Oxygen on Mo/HZSM-5: A Study on the Interaction between Mo Species and HZSM-5 by Using ²⁷Al and ²⁹Si MAS NMR. *J. Mol. Catal. A: Chem.* **1997**, *120*, 257–265.
- (30) Córdoba, L. F.; Fuentes, G. A.; de Correa, C. M. Characterization of Bimetallic Pd/Co-HMOR Used for the CH₄-SCR of NO_x. *Microporous Mesoporous Mater.* **2005**, *77*, 193–201.
- (31) Delabie, A.; Pierlot, K.; Groothaert, M. H.; Weckhuysen, B. M.; Schoonheydt, R. A. The Siting of Cu(II) in Mordenite: A Theoretical Spectroscopic Study. *Phys. Chem. Chem. Phys.* **2002**, *4*, 134–145.
- (32) Putluru, S. S. R.; Jensen, A. D.; Riisager, A.; Fehrmann, R. Alkali Resistant Fe-Zeolite Catalysts for SCR of NO with NH₃ in Flue Gases. *Top. Catal.* **2011**, *54*, 1286–1292.
- (33) Kapustin, G. I.; Brueva, T. R.; Klyachko, A. L.; Beran, S.; Wichterlova, B. Determination of the Number and Acid Strength of Acid Sites in Zeolites by Ammonia Adsorption: Comparison of Calorimetry and Temperature-Programmed Desorption of Ammonia. *Appl. Catal.* **1988**, *42*, 239–246.
- (34) Lobree, L. J.; Hwang, I. C.; Reimer, J. A.; Bell, A. T. Investigations of the State of Fe in H-ZSM-5. *J. Catal.* **1999**, *186*, 242–253.
- (35) Brown, D. R.; Rhodes, C. N. Brønsted and Lewis Acid Catalysis with Ion-Exchanged Clays. *Catal. Lett.* **1997**, *45*, 35–40.
- (36) Lezcano-Gonzalez, I.; Deka, U.; Arstad, B.; Van Yperen-De Deyne, A.; Hemelsoet, K.; Waroquier, M.; Van Speybroeck, V.; Weckhuysen, B. M.; Beale, A. M. Determining the Storage, Availability and Reactivity of NH₃ within Cu-Chabazite-Based Ammonia Selective Catalytic Reduction Systems. *Phys. Chem. Chem. Phys.* **2014**, *16*, 1639–1650.
- (37) Benaliouche, F.; Boucheffa, Y.; Thibault-Starzyk, F. In Situ FTIR studies of Propene Adsorption over Ag- and Cu-Exchanged Y Zeolites. *Microporous Mesoporous Mater.* **2012**, *147*, 10–16.
- (38) Suzuki, K. Quantitative Measurements of Brønsted Acidity in Zeolites by Ammonia IRMS–TPD Method. Doctoral Thesis, Tottori University, Tottori, Japan, 2009.
- (39) Cheung, P.; Bhan, A.; Sunley, G. J.; Iglesia, E. Selective Carbonylation of Dimethyl Ether to Methyl Acetate Catalyzed by Acidic Zeolites. *Angew. Chem., Int. Ed.* **2006**, *45*, 1617–1620.
- (40) Jiang, Y.; Hunger, M.; Wang, W. On the Reactivity of Surface Methoxy Species in Acidic Zeolite Catalysts. *J. Am. Chem. Soc.* **2006**, *128*, 11679–11692.
- (41) Lercher, J. A.; Gründling, C.; Eder-Mirth, G. Infrared Studies of the Surface Acidity of Oxides and Zeolites Using Adsorbed Probe Molecules. *Catal. Today* **1996**, *27*, 353–376.
- (42) Benco, L.; Bucko, T.; Hafner, J.; Toulhoat, H. Ab Initio Simulation of Lewis Sites in Mordenite and Comparative Study of the

Strength of Active Sites via CO Adsorption. *J. Phys. Chem. B* **2004**, *108*, 13656–13666.

(43) Gupta, N. M.; Kamble, V. S.; Annaji Rao, K.; Iyer, R. M. Co Adsorption–Desorption Properties of Cation-Exchanged NaX Zeolite and Supported Ruthenium. *J. Catal.* **1989**, *120*, 432–443.

(44) Rice, M. J.; Chakraborty, A. K.; Bell, A. T. Theoretical Studies of the Coordination and Stability of Divalent Cations in ZSM-5. *J. Phys. Chem. B* **2000**, *104*, 9987–9992.

(45) Li, B.; Xu, J.; Han, B.; Wang, X.; Qi, G.; Zhang, Z.; Wang, C.; Deng, F. Insight into Dimethyl Ether Carbonylation Reaction over Mordenite Zeolite from in-Situ Solid-State NMR spectroscopy. *J. Phys. Chem. C* **2013**, *117*, 5840–5847.

(46) Boronat, M.; Martínez, C.; Corma, A. Mechanistic Differences between Methanol and Dimethyl ether Carbonylation in Side Pockets and Large Channels of Mordenite. *Phys. Chem. Chem. Phys.* **2011**, *13*, 2603–2612.

(47) Liu, J. L.; Xue, H. F.; Huang, X. M.; Wu, P. H.; Huang, S. J. Stability Enhancement of H-Mordenite in Dimethyl Ether Carbonylation to Methyl Acetate by Pre-adsorption of Pyridine. *Chin. J. Catal.* **2010**, *31*, 729–738.